

# Superscaling of Inclusive Electron Scattering from Nuclei

T. W. Donnelly

Center for Theoretical Physics, Laboratory for Nuclear Science  
and Department of Physics  
Massachusetts Institute of Technology  
Cambridge, Massachusetts 02139-4307, USA

Ingo Sick

Departement für Physik und Astronomie, Universität Basel  
CH4056 Basel, Switzerland

We investigate the degree to which the concept of superscaling, initially developed within the framework of the relativistic Fermi gas model, applies to inclusive electron scattering from nuclei. We find that data obtained from the low energy loss side of the quasielastic peak exhibit the superscaling property, *i.e.* the scaling functions  $f(\psi')$  are not only independent of momentum transfer (the usual type of scaling: scaling of the first kind), but coincide for  $A \geq 4$  when plotted versus a dimensionless scaling variable  $\psi'$  (scaling of the second kind). We use this behavior to study as yet poorly understood properties of the inclusive response at large electron energy loss.

## 1 Introduction

The applications of scaling and dimensional analysis have been important tools for the development of new insights in physics. Scaling in scattering experiments is observed in processes where a weakly interacting probe scatters from constituents bound in a composite system and a constituent is ejected quasifreely from the system. The (unpolarized) inclusive response functions, determined by observing only the scattered probe, in addition to depending on the scattering angle, in general depend explicitly on only two more independent variables — the energy  $\omega$  and momentum  $\mathbf{q}$  transferred by the probe to the constituent. In the asymptotic regime of large  $q = |\mathbf{q}|$  and  $\omega$ , however, when appropriately divided by the elementary probe-constituent cross section, the responses are (approximately) functions of only a *single* variable  $z = z(q, \omega)$ , with  $z$  in turn a function of  $q$  and  $\omega$ . This functional independence of the so-called scaling function on the momentum transfer (which sets the scale in the scattering) is known as scaling

and is seen as a signature that the scattering occurred between the probe and the specific elementary constituent of the target, rather than arising from some other process such as scattering from different constituents. To distinguish this behavior from the additional scaling that forms the focus of the present work we call the usual independence of momentum transfer *scaling of the first kind*. Various choices for the function  $z(q, \omega)$  can be motivated on the basis of the kinematics of the probe-constituent elastic scattering process — several such choices are discussed in this work. Expressed in terms of a scaling function, the inclusive cross sections can be related to the momentum distribution (more generally, to the spectral function) of the constituents in the target.

In the last 20 years or so, the concept of  $y$ -scaling in scattering of high-energy electrons from nuclei has been actively pursued [1]. For  $y$ -scaling the focus is on protons and neutrons in nuclei as the “elementary” constituents. Typically, when three-momenta of  $q > 500$  MeV/c and energies at or somewhat below the quasielastic peak position  $\omega \approx (q^2 + m_N^2)^{1/2} - m_N$ , where  $m_N$  is the nucleon mass, are transferred from the electron to the nucleus via exchange of a virtual photon, a nucleon is ejected from the nucleus in a reasonably “quasifree” manner. Namely, the nucleon leaves the nucleus with a high enough energy that the process can be treated approximately as having occurred without strong effects from final-state interactions (FSI). Under the appropriate kinematical conditions (to which we return below) the cross section can be written as a product of the elementary electron-nucleon elastic cross section times a function  $F$ . It has been shown theoretically and verified experimentally that at large momentum transfers the appropriately defined function  $F$  depends only on a single variable  $y = y(q, \omega)$ , itself a function of  $q$  and  $\omega$ ; here  $y$  is a particular choice for the general function  $z$  referred to above (see also the next section). The scaling function so obtained asymptotically contains interesting information about the dynamical properties of the nuclear ground state, and the fact that scaling does occur provides very useful information about the reaction mechanism itself.

Indeed, scaling in electron-nucleus scattering is a special case of a more general phenomenon [2] occurring in various areas of physics that deal with inelastic scattering of a weakly interacting probe from a many-body system in which  $q$  and  $\omega$  are transferred to a single constituent in the target system. Examples are found in the scattering of keV electrons from electrons bound in atoms [3], in the scattering of eV neutrons from atoms in solids or liquids [4] and in the scattering of GeV electrons from quarks in the nucleon [5]. Despite the extraordinary range of energy and momentum transfers for which these reactions have been studied, the conceptual ideas used to describe the scaling phenomena in these different fields have many features in common.

For electron-nucleus scattering, the topic of particular interest to this paper, scaling was already implicit in the early theoretical studies of electron-nucleus

quasielastic scattering [6] when treated in terms of the non-relativistic Fermi gas model; the cross section could be reduced to a function of a single variable multiplied by the elementary e-N elastic cross section. For treating electron scattering explicitly in terms of  $y$ -scaling, the seminal idea originated with the work of West [2]. Early theoretical work was also undertaken by Kawazoe [7]. At that time, however, few data were available and where they did exist they were restricted to a narrow kinematical range at low energy. Conclusive observation of the asymptotic  $q$ -independence of  $F$  for inclusive scattering became possible with the availability of data that spanned a large range of  $q$  and  $\omega$  and was presented by Sick *et al.* [8] for  ${}^3\text{He}$ . Subsequent work [9, 10] placed the theoretical foundations of scaling on reasonably firm ground, specifically addressing a variety of issues such as the role of the restrictions imposed by the nature of the  $(A - 1)$  system excitation spectrum and recoil-nucleon FSI [11]. A summary of the various aspects of conventional (first kind) scaling has been given in the review paper of Day *et al.* [1].

Much of the previous work has concentrated on the study of the scaling properties of the response in the low- $\omega$  tail of the quasielastic peak; in this region the scaling function is sensitive to components of the spectral function at large initial nucleon momenta. Particular emphasis was placed on light nuclei  $A \leq 4$  where the scaling approach works particularly well and where sophisticated calculations of ground-state nuclear wave functions and hence spectral functions are available for theoretical studies of the scaling properties.

In the present paper, we explore a different aspect of scaling. Rather than concentrating on the response of individual nuclei, we compare the scaling function of *different nuclei* with  $A \geq 4$ , and study the degree to which these scaling functions are the *same* — we call such behavior scaling of the *second kind*. The motivation is to explore the degree to which the concept of *superscaling* introduced by Alberico *et al.* [12] when studying the properties of the Relativistic Fermi Gas (RFG) model, that is, scaling of both the first and second kinds, is applicable to nuclei. A presentation in condensed form of some of this analysis is available in Ref. [13].

Here we study superscaling using a large body of inclusive scattering data. While we employ the RFG model to motivate the choice of the scaling variable, only minimal use of this model is subsequently made in interpreting the data as the actual dynamical physics content in the problem is undoubtedly more complex than the RFG model can be expected to address. The RFG does, however, offer a physical scale — the Fermi momentum — that can be used to make both the scaling variable and scaling function dimensionless. The emphasis of the present paper therefore is on superscaling as observed in the experimental data, and on the physics one can deduce from this scaling property. Here (in Sec. 2 and the Appendix) we also provide discussion in depth of the choices made for the scaling

variables, their limiting expressions and the inter-relationships amongst them.

Scaling of the second kind and superscaling were actually implicit although unrecognized in the early work of [14] in which quasielastic scattering was studied at one value of momentum transfer for a range of nuclei  $A = 6\text{--}208$ . The data at energy loss below the maximum of the quasielastic peak could be explained in the Fermi gas model, an observation that implies that scaling of the second kind did occur. No scaling analysis of the data was performed, however.

Using modern data we find that the superscaling idea works very well in the region below the quasielastic peak, as discussed in Sec. 3 (see also [13]). However, some breaking of superscaling does occur, and in the present work we use such deviations to elucidate some of the as yet not well understood features observed in the various measurements of the quasielastic response. In particular, in Sec. 4 we focus on the difference between the longitudinal and transverse responses in the region of the quasielastic peak, and the properties of the contributions that fill in the “dip” between the quasielastic and  $\Delta$  peaks — a region which has presented a puzzle for a long time [14].

Following this introduction we proceed in Sec. 2 to discuss the relevant formalism involved in scaling of the first and second kinds for the cross sections, relegating some details to an Appendix. Then in Sec. 3 we discuss the results of analyzing the existing data on quasielastic electron scattering, including recent results from TJNAF [15], to test the idea of superscaling. Subsequently in Sec. 4 we specialize the formalism and discussion of the data to a treatment of the individual longitudinal and transverse responses. We end in Sec. 5 with the conclusions to be drawn from the present study and with some discussion of the questions that must still be regarded as open ones in studies of quasielastic electron scattering from nuclei at intermediate energies.

## **2 Scaling of Cross Sections: Formalism**

Let us begin by repeating and extending some of the arguments that underlie the concept of  $y$ -scaling of the unseparated cross sections; these form part of the basis of the discussions of superscaling that follow, and several identities and relationships amongst the variables involved are presented for the first time. In the usual approach to inclusive electron scattering in the quasielastic regime one assumes that the dominant process is impulsive one-body knockout of nucleons together with contributions from two-body processes that play a role when the normally dominant process is suppressed. Of course, for the ideas of scaling to be applicable one must avoid the regime of low energy and momentum transfers where strong FSI effects (including Pauli blocking, collective behavior in the final states, etc.) are felt. Also the distortion of the initial and final electron wave

functions moving in the Coulomb field of the nucleus must be addressed (at least for heavy nuclei and low electron energy) for the scaling analysis to be clear.

The usual approach is the following: One starts from the  $(e, e'p)$  and  $(e, e'n)$  cross sections which may be written as functions of the 3-momentum transfer  $q = |\mathbf{q}|$  and energy transfer  $\omega$ , the electron scattering angle  $\theta_e$ , the azimuthal angle  $\phi_N$  between the planes in which the electrons lie and in which the momentum transfer and the outgoing nucleon lie, and two variables specifying the remaining kinematics of the outgoing nucleon. For the latter one may use the 3-momentum of the nucleon  $p_N = |\mathbf{p}_N|$  or its energy  $E_N = (m_N^2 + p_N^2)^{1/2}$  and its polar angle  $\theta_N$ , the angle between  $\mathbf{q}$  and  $\mathbf{p}_N$ . Alternatively one may use the magnitude of the missing-momentum  $p = |\mathbf{p}| = |\mathbf{p}_N - \mathbf{q}|$  and a variable to characterize the degree of excitation of the residual system; for the latter we use

$$\mathcal{E}(p) \equiv \sqrt{(M_{A-1})^2 + p^2} - \sqrt{(M_{A-1}^0)^2 + p^2} \geq 0, \quad (1)$$

where  $m_N$  is the nucleon mass,  $M_{A-1}$  is the (in general) excited recoiling system's mass, while  $M_{A-1}^0$  is that system's mass when in its ground state. The target mass is denoted  $M_A^0$  and the separation energy relates three of the masses in the following way:  $E_S \equiv M_{A-1}^0 + m_N - M_A^0 \geq 0$ . The variable  $\mathcal{E}$  is essentially the familiar missing-energy minus the separation energy.

The strategy in the usual scaling analyses is to determine the smallest value of missing-momentum  $p$  that can occur for the smallest possible value of missing-energy (i.e.,  $\mathcal{E} = 0$ ), since there, at least for kinematics not too far removed from the quasielastic peak, one might expect to have the largest contributions from the underlying nuclear spectral function — see, however, the discussions at the end of this section. This smallest value of  $p$  is traditionally defined to be  $y$  ( $-y$ ) for  $\omega$  larger (smaller) than its value at the quasielastic peak. Thus one may use  $(q, y)$  rather than  $(q, \omega)$  as the two variables together with  $\theta_e$  upon which the inclusive cross section depends. In the Appendix we give complete expressions for  $y$  and for the largest value of  $p$  that may be reached for given  $q$  and  $\omega$ ; here we give an expression only for  $y$  in the limit where  $M_{A-1}^0 \rightarrow \infty$ , as for all but the very lightest nuclei this is an excellent approximation:

$$y_\infty = \sqrt{\tilde{\omega}(2m_N + \tilde{\omega})} - q, \quad (2)$$

where  $\tilde{\omega} \equiv \omega - E_S$ . Corrections of order  $(M_{A-1}^0)^{-1}$  are also given in the Appendix (see Eq. (40)).

Focusing now on the region  $y < 0$ , the most common approach to  $y$ -scaling (see, for example, [1]) is then to evaluate the single-nucleon cross section at the lowest values of  $(p, \mathcal{E})$  that can be reached for given values of  $q$  and  $y$  — in the scaling region these are  $p = -y$  and  $\mathcal{E} = 0$  — and then to divide the inclusive

cross section by this quantity to define a function of  $q$  and  $y$ :

$$F(q, y) \equiv \frac{d^2\sigma/d\Omega_e d\omega}{\tilde{\sigma}_{eN}(q, y; p = -y, \mathcal{E} = 0)}. \quad (3)$$

For the single-nucleon cross section it is common practice to use the cc1 prescription of De Forest [16] with the form factors parametrized as in [17]. In the Appendix we provide the complete expressions for the cross section and indicate the degree to which the struck nucleon in Plane-Wave Impulse Approximation (PWIA) is off-shell. In PWIA one has

$$F(q, y) = 2\pi \int_{-y}^Y p dp \tilde{n}(q, y; p), \quad (4)$$

involving the integral

$$\tilde{n}(q, y; p) = \int_0^{\mathcal{E}_M} d\mathcal{E} \tilde{S}(p, \mathcal{E}) \quad (5)$$

whose upper limit is approximately given by

$$\mathcal{E}_M(q, y; p) \cong \sqrt{m_N^2 + (q + y)^2} - \sqrt{m_N^2 + (q - p)^2} \quad (6)$$

$$\cong m_N + \tilde{\omega} - \sqrt{m_N^2 + (q - p)^2} \quad (7)$$

using Eq. (2). Here again we have taken the limit where  $M_{A-1}^0 \rightarrow \infty$ , relegating the exact expressions to the Appendix (see Eqs. (42)). At high enough values of  $q$  one seeks the  $y$ -scaling behavior: namely, if the inclusive response scales then  $F$  becomes only a function of  $y$ ,

$$F(q, y) \xrightarrow{q \rightarrow \infty} F(y) \equiv F(\infty, y). \quad (8)$$

Scaling has also been approached from a different point of view using as a starting point the RFG model [12, 18]. The strategy there is to provide a form similar to Eq. (3) such that in this model exact scaling is obtained. As seen in [18] the variable

$$y_{RFG} = m_N \left( \lambda \sqrt{1 + 1/\tau} - \kappa \right) \quad (9)$$

naturally emerges. Here, as in many past studies, we employ dimensionless versions of  $q$ ,  $\omega$  and  $|Q^2|$ :  $\kappa \equiv q/2m_N$ ,  $\lambda \equiv \omega/2m_N$  and  $\tau \equiv |Q^2|/4m_N^2 = \kappa^2 - \lambda^2$ . Below we show how to inter-relate the variables  $y$  and  $y_{RFG}$ . As also discussed in the above-cited work, a dimensionless scaling variable  $\psi$  is strongly motivated

by the RFG model. In the Appendix we give the exact expression for  $\psi$  (see Eq. (52)), whereas for most purposes the following approximations are excellent:

$$\psi = \frac{y_{RFG}}{k_F} \left[ 1 + \mathcal{O}[\eta_F^2] \right] \quad (10)$$

$$\cong \frac{1}{\eta_F} \left[ \lambda \sqrt{1 + 1/\tau} - \kappa \right], \quad (11)$$

where  $k_F$  is the Fermi momentum and  $\eta_F = k_F/m_N$  its dimensionless counterpart. Typically  $\eta_F$  is small, growing from 0.06 for deuterium to about 0.3 for the heaviest nuclei, and thus expansions such as those above are usually quite good, since they neglect terms only of order  $\eta_F^2$ . An alternative approximation for  $\psi$  that also proves useful to introduce is the following:

$$\psi = \psi_0 \left[ 1 + \sqrt{1 + 1/4\kappa^2} \frac{1}{2} \eta_F \psi_0 + \mathcal{O}[\eta_F^2] \right], \quad (12)$$

where now the good (but not as good) variable

$$\psi_0 \equiv \frac{2}{\eta_F} \left[ \sqrt{\lambda(1 + \lambda)} - \kappa \right] \quad (13)$$

occurs and the result in Eq. (12) receives linear (rather than quadratic) corrections when written in terms of  $\psi_0$ .

The RFG analog of Eq. (3) is

$$F(\kappa, \psi) \cong \frac{d^2\sigma/d\Omega_e d\omega}{\sigma_M \left[ \frac{\kappa}{2\tau} v_L \tilde{G}_E^2 + \frac{\tau}{\kappa} v_T \tilde{G}_M^2 \right]}, \quad (14)$$

where we have made use of the usual lepton kinematical factors  $v_L$  and  $v_T$  and the approximations for the single-nucleon responses  $G_L$  and  $G_T$  which involve  $\tilde{G}_E^2 \equiv ZG_{Ep}^2 + NG_{En}^2$  with  $\tilde{G}_M^2$  defined similarly (see Eqs. (49) and (53–55)). Note that relativistic factors involving the difference between  $\kappa^2$  and  $\tau$  in Eq. (14) are very important to retain when studying quasielastic scattering at high momentum transfers.

Before carrying these ideas over to an analysis of the data, it is useful to bridge the gap between the usual  $y$ -scaling approach and the  $\psi$ -scaling ideas contained in the RFG (see also [18]). First, let us use the  $y$  variable to define its dimensionless counterpart,

$$\Upsilon \equiv y/k_F \quad (15)$$

and from Eq. (2) its approximate form,

$$\Upsilon_\infty \equiv y_\infty/k_F = \frac{2}{\eta_F} \left[ \sqrt{\tilde{\lambda}(1 + \tilde{\lambda})} - \kappa \right], \quad (16)$$

where  $\tilde{\lambda} \equiv \tilde{\omega}/2m_N$ . Clearly the two approaches will yield rather similar results, since

$$\psi_0 = \Upsilon_\infty(E_s = 0), \quad (17)$$

with corrections to  $\Upsilon$  coming from the finite-mass effects discussed in the Appendix (see Eq. (40)) and to  $\psi$  from the  $\eta_F$ -dependent terms in Eq. (12) (see also below). The  $y$ - and  $\Upsilon$ -variables build in the kinematics of nucleon knockout and recognize the initial-state separation energy  $E_s$ ; however, they do not take into account the missing-energy dependence in the cross section. On the other hand, the  $\psi$ -variable is constructed from the RFG model where  $A \rightarrow \infty$  at constant density (and thus contains no finite-mass dependences), although, as discussed in more detail below, it does reflect some of the missing-energy content in the problem (see also [19]).

Thus, each approach has its own merits. To bridge the gap at least partially, it is useful to shift the energy  $\omega$  to

$$\omega' \equiv \omega - E_{shift} \quad (18)$$

by an amount  $E_{shift}$  to be chosen empirically (see the next section where we discuss the choices made for the shift and allow  $E_{shift}$  to take on values other than  $E_s$ , the separation energy). In the familiar  $y$ -scaling analysis, already one usually does not use  $E_s$  as would be demanded if strictly adhering to the PWIA, but rather lets the shift “float” to allow the quasielastic peak to occur in the correct position. This usually results in a somewhat larger value for the shift and probably reflects the fact that implicitly one is trying to build in some aspects of the initial-state physics such as the average removal energy — the average of the separation energies of the various shells making up the nuclear ground state — but also some aspects of FSI which can also produce a shift in the position of the quasielastic peak. Actually, the difference between the strict interpretation as a separation energy and the empirical value that emerges is typically rather small.

We then adopt the same strategy when proceeding from the RFG starting point and introduce dimensionless variables as above,  $\lambda' \equiv \omega'/2m_N$  and  $\tau' \equiv \kappa^2 - \lambda'^2$ , so that in parallel with Eq. (13) we have

$$\psi_0' \equiv \psi_0[\lambda \rightarrow \lambda'] = \frac{2}{\eta_F} \left[ \sqrt{\lambda'(1 + \lambda')} - \kappa \right] = \Upsilon_\infty(\tilde{\lambda} = \lambda') \quad (19)$$

and Eq. (12)

$$\psi' \equiv \psi[\lambda \rightarrow \lambda'] = \psi_0' \left[ 1 + \sqrt{1 + 1/4\kappa^2} \frac{1}{2} \eta_F \psi_0' + \mathcal{O}[\eta_F^2] \right]. \quad (20)$$



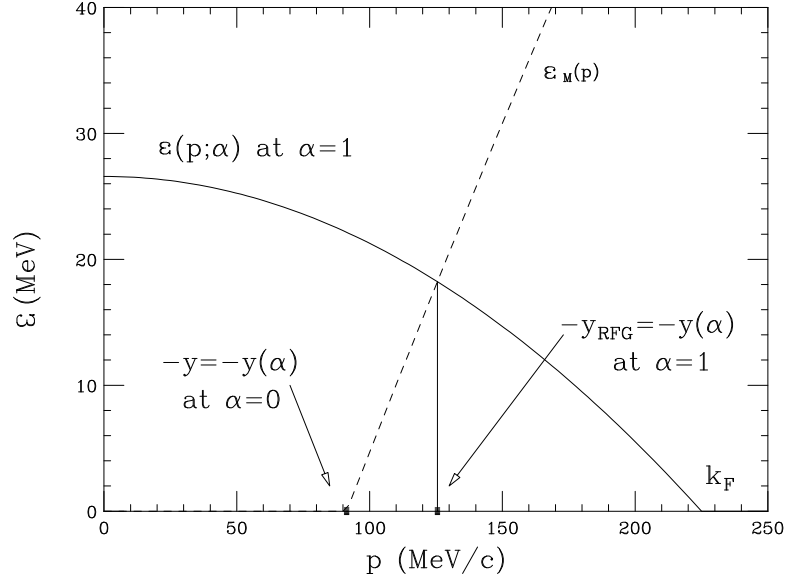


Figure 1: Missing-energy versus missing-momentum. The various curves are described in the text; they are shown for  $k_F = 225$  MeV/c,  $E_{shift} = 20$  MeV,  $q = 700$  MeV/c and  $\omega = 200$  MeV.

A simple extension of the strict RFG model should help in providing an understanding of the missing-energy content retained in defining a scaling variable. The RFG has a spectral function which is non-zero along the line:

$$\mathcal{E}_{RFG}(p) = \sqrt{k_F^2 + m_N^2} - \sqrt{p^2 + m_N^2} \quad (21)$$

that “on the average” [19] incorporates the shell structure of a typical (heavy) nucleus. Instead let us use

$$\mathcal{E}(p; \alpha) \equiv \alpha \mathcal{E}_{RFG}(p), \quad (22)$$

such that when  $\alpha = 1$  we recover the RFG model, but when  $\alpha = 0$  we have  $\mathcal{E} = 0$ , the constraint used in defining the familiar  $y$  variable (see Eq. (38) in the Appendix). In Fig. 1 we show  $\mathcal{E}(p; 1)$  together with  $\mathcal{E}_M(p)$  from Eqs. (6,7) at  $q = 700$  MeV/c and  $\tilde{\omega} = 180$  MeV — namely for typical kinematics for the low- $\omega$  side of the quasielastic peak. As in the RFG model (see [18]), the intersection of the two curves occurs at the value of missing-momentum  $p$  that defines the scaling variable. For  $\alpha = 0$  this occurs at  $-y$ , the usual scaling variable given approximately by  $y_\infty$  in Eq. (2) (for simplicity here we have taken  $\omega' = \tilde{\omega}$ ); for  $\alpha = 1$  it occurs at  $-y_{RFG}$  given in Eq. (9) (but, of course, with  $\omega$  shifted). More generally one obtains something very similar to Eqs. (12) and (20), namely

$$y(\alpha) = y_\infty \left[ 1 + \alpha \sqrt{1 + 1/4\kappa^2} \frac{1}{2} \eta_F \psi_0' + \mathcal{O}[\eta_F^2] \right]. \quad (23)$$

Clearly what emerges is the following: the term in Eq. (20) containing a first-order correction to the “minimal” approximation to the shifted RFG scaling variable,  $\psi_0'$ , is the one above involving  $\alpha$ . When  $\alpha = 0$  (the usual  $y$  definition) no missing-energy dependence is taken into account, whereas with  $\alpha \neq 0$  (as in the RFG) some average dependence on  $\mathcal{E}$  is incorporated.

Indeed, if circumstances warranted, it is straightforward to generalize these ideas to devise still more scaling variables that build in the best features of both the traditional PWIA-motivated extreme and the RFG model extreme, or to go beyond in attempting to take into account whatever we know about the missing-energy dependence of realistic spectral functions. However, as the results given in the next section show, such fine-tuning is apparently not needed at the present stage of our understanding of superscaling.

Finally, having obtained dimensionless scaling variables  $\psi$ ,  $\psi'$  and  $\Upsilon$  (together with approximations to them, as discussed above), we introduce a *dimensionless version of the scaling function* as suggested by the RFG model [12, 18]

$$f \equiv k_F \times F. \quad (24)$$

Not only does the RFG model contain scaling of the *first kind* so that  $f$  (or  $F$ ) becomes independent of  $q$  at high momentum transfers, retaining dependence only on the scaling variable  $\psi$ , but it also contains scaling of the *second kind* wherein  $f$  is independent of  $k_F$  to leading order in  $\eta_F^2$ . What results for this model is

$$f_{RFG}(\psi) = \frac{3}{4}(1 - \psi^2)\theta(1 - \psi^2) \left[ 1 + (\eta_F\psi/2)^2 + \dots \right]. \quad (25)$$

When both types of scaling occur as they do for the RFG model we call the behavior *superscaling*. In the next section we proceed to examine the degree to which scaling of the various kinds does or does not occur for measured unseparated cross sections.

### 3 Scaling of Cross Sections: Results

In this section we use the unseparated electron-nucleus inclusive scattering data presently available to test the idea of superscaling for kinematics below the quasielastic peak and also try to add some insight into the various reasons which lead to the well-known fact that at large electron energy loss non-scaling behavior is observed. We restrict our attention to nuclei heavier than  ${}^3\text{He}$ , as the lightest nuclei are known to have momentum distributions that are very far from the “universal” one which is at the basis of the superscaling idea.

Data on inclusive electron-nucleus scattering for a series of nuclei ( $A = 4$ –208), but only one set of kinematics, were obtained early on by Whitney *et al.* [14].

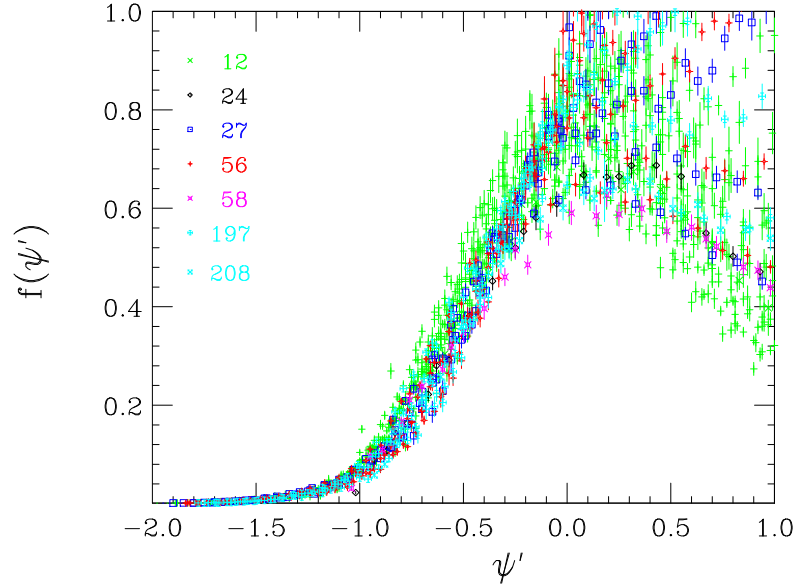


Figure 2: Scaling function  $f(\psi')$  as function of  $\psi'$  for all nuclei  $A \geq 12$  and all kinematics. The values of  $A$  corresponding to different symbols are shown in the insert.

For helium, additional data at low  $q$  were measured by Zghiche *et al.*, Dytman *et al.*, Meziani *et al.*, Sealock *et al.* and von Reden *et al.* [14, 20]-[24]; high- $q$  data were obtained by Day *et al.* and Rock *et al.* [25, 26]. For carbon, low momentum transfer data are available from experiments performed by Barreau *et al.*, Baran *et al.* and O’Connell *et al.* [27]-[30]; at high  $q$  cross sections are available from the experiments of Day *et al.* and Heimlich *et al.* [25, 31]. For oxygen an experiment has been performed by Anghinolfi *et al.* [32]. For medium-weight nuclei the data available include those for aluminum at high  $q$  measured by Day *et al.* [25], and the ones for calcium measured by Deady *et al.*, Meziani *et al.*, Yates *et al.* and Williamson *et al.* [33]-[36] at low  $q$ . For iron experiments have been performed by Altemus *et al.*, Meziani *et al.*, Baran *et al.*, Sealock *et al.* and Hotta *et al.* at low  $q$  [37, 34, 29, 23, 38]; at high  $q$  measurements have been made by Day *et al.* and Chen *et al.* [25, 39]. For heavy nuclei inclusive cross sections have been measured by Day *et al.* for gold at high  $q$  [25], and by Zghiche *et al.*, Blatchley *et al.* and Sealock *et al.* for nuclei between tungsten and uranium at low  $q$  [20, 40, 23].

Not all of these data can be used, however, as some have not been corrected for radiative effects, are known to have problems such as “snout scattering” or have a floating normalization; some data are only available in the form of figures, but not as numerical values, and thus are not useful in the present context.

To begin with (see also [13]), we have taken the available data for the nuclei

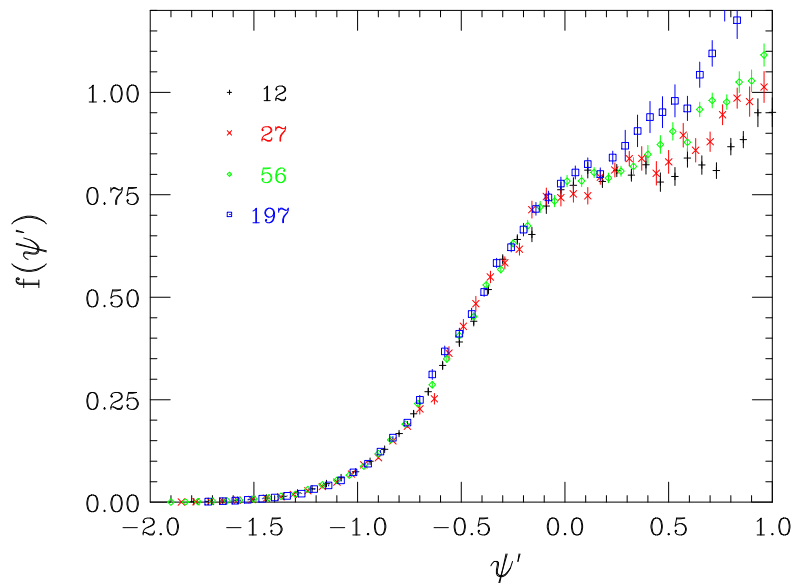


Figure 3: Scaling function for C, Al, Fe, Au and fixed kinematics ( $q \approx 1000$  MeV/c).

$A = 12 \dots 208$  that meet our criteria for inclusion and have analyzed them in terms of scaling in the variable  $\psi'$ . Since  $\psi'$  is defined in Eqs. (19,20) in terms of the Fermi momentum, appropriate values of  $k_F$  had to be selected: specifically, we use 220, 230, 235 and 240 MeV/c for C, Al, Fe, Au, with intermediate values for the intermediate nuclei. The definition of the scaling variable also involves the choice of an appropriate “shift” energy (see Eq. (18)). This energy accounts for the effects of both the binding in the initial state and the interaction strength in the final state. In practice we use an energy that goes from 15 to 25 MeV for nuclei C...Au; the results are quite insensitive to the exact choice.

Figure 2 shows the scaling function  $f(\psi')$  defined in Eq. (24) for all kinematics (energies, angles, momentum transfers) and all available nuclei meeting our selection criteria. We observe reasonably successful superscaling behavior for values of  $\psi' < 0$ , while for  $\psi' > 0$  the superscaling property is badly violated. The latter is to be expected, as there processes other than quasielastic scattering — meson-exchange currents (MEC),  $\Delta$ -excitation, deep inelastic scattering — contribute to the cross section, whereas the scaling as discussed in this paper only applies to quasielastic scattering.

In order to understand better the deviations from ideal scaling, below we take different cuts through the data. The presently available data unfortunately involve strong correlations in the kinematics employed: as the momentum transfer increases, the longitudinal (L) to transverse (T) cross section ratio for quasielastic

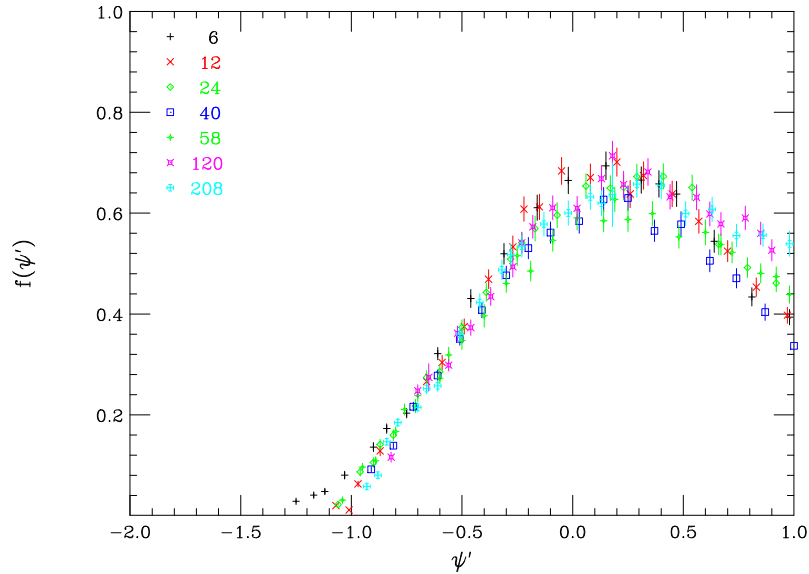


Figure 4: Scaling function for Li, C, Mg, Ca, Ni, Sn, Pb and fixed kinematics ( $q \approx 460$  MeV/c).

scattering decreases. At the same time, the higher- $q$  data are taken at more forward angles. A separation of the influence of the different driving factors such as  $q$ , L/T ratio and  $A$ -dependence is therefore not straightforward.

In order to disentangle some of these less-than-perfect superscaling effects at  $\psi' < 0$ , we show in Fig. 3 the function  $f(\psi')$  for the series of nuclei  $A = 12 \dots 197$ , but for fixed kinematics (electron energy 3.6 GeV, scattering angle  $16^\circ$ , where  $q$  varies only mildly over the range shown). The quality of scaling of the second kind in the region  $\psi' < 0$  is quite amazing, showing that insofar as the removal of the  $A$ -dependence is concerned the superscaling works extremely well and, importantly, that the deviations from superscaling observed in Fig. 2 for  $\psi' < 0$  do *not* arise from the  $A$ -dependence. The scaling of the second kind works very well.

As similar quality of superscaling is found when analyzing other momentum transfers where a set of data for  $A = 6 \dots 208$  is available. As an example in Fig. 4 we show the lower- $q$  data from the experiment of Whitney *et al.* [14] taken at 500 MeV electron energy and  $60^\circ$  scattering angle.

Figure 5 shows the same data as those used in Fig. 3 on a logarithmic scale, demonstrating that the superscaling property extends to large negative values of  $\psi'$ , values which in PWIA correspond to large momenta for the initial nucleon. A priori, this feature is not predicted within the RFG model used to motivate the choice of  $\psi'$ . It can be understood, however, from the theoretical results for

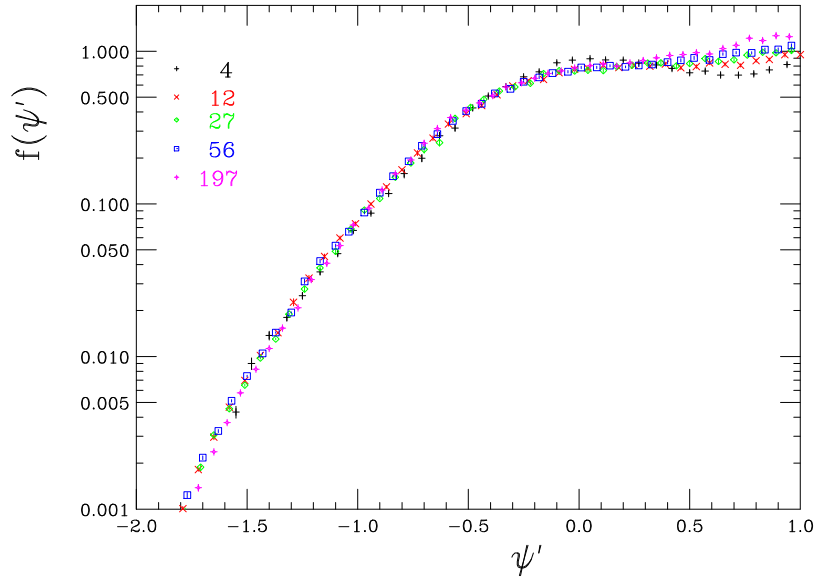


Figure 5: Scaling function for nuclei  $A = 4$ – $197$  and fixed kinematics ( $q \approx 1000$  MeV/c) on a logarithmic scale.

the momentum distribution of nuclear matter as a function of the nuclear matter density where, for different nuclear matter densities, the tail of the momentum distribution is a near-universal function of  $k/k_F$  [41]. Since at large  $k$  we deal with short-range properties of the nuclear wave function [42], for finite nuclei and large momenta we can employ the Local Density Approximation (LDA), within which the nuclear momentum distribution (spectral function) is then a weighted average over the corresponding nuclear matter distributions. This means that the large-momentum tail of the nuclear momentum distribution also scales with  $k_F$ , a dependence that is removed when using  $\psi'$ .

In order to emphasize the quality of this superscaling in the tail, in Fig. 5 we have also included the data for  ${}^4\text{He}$  which were taken under the same kinematical conditions as the other sets ( $k_F = 200$  MeV/c,  $E_{shift} = 15$  MeV). While at  $\psi' = 0$  the superscaling function  $f(\psi')$  for  ${}^4\text{He}$  is about 15% higher than for heavier nuclei, a consequence of the sharper peak of the momentum distribution  $n(k)$  at  $k \approx 0$  for such a light nucleus, the scaling function for  ${}^4\text{He}$  agrees perfectly with the one for heavier nuclei when  $\psi' < -0.3$ . This reflects the fact that the tail of the momentum distribution  $n(k)$  at large  $k$  is determined by the short-range properties of the N–N interaction.

Part of the  $A$ -dependent increase of  $f(\psi')$  at large  $\psi'$  results from the increase of  $k_F$  in proceeding from light to heavy nuclei. This amounts to an increase of the width of the quasielastic peak (i.e., before scaling with  $k_F$ ) and a correspond-

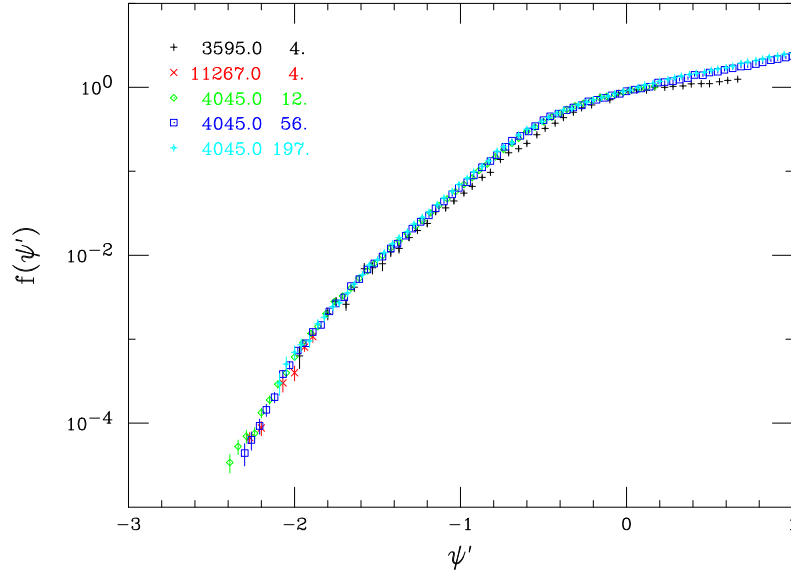


Figure 6: Scaling function for nuclei  $A = 4$ –197 at  $q \approx 1650$  MeV/c. The 4.405 GeV data have been taken at  $23^\circ$  scattering angle, the  $^4\text{He}$  data at  $25^\circ$  and  $8^\circ$ .

ingly increased overlap with non-quasifree scattering processes ( $\Delta$ -excitation,  $\pi$ -production,...). At the same time, the increasing average density of the heavier nuclei also leads to an increase in contributions of two-body processes such as MEC which are strongly density-dependent [43]. This, however, appears not to be the only cause for the rise (see the discussions in Sec. 4).

Recently, the inclusive scattering data on C, Fe and Au have been extended to more negative values of  $\psi'$  by an experiment performed at TJNAF [15]. The higher product of beam current and spectrometer solid angle allowed Arrington *et al.* to measure cross sections a hundred times smaller than previously accessible. In Fig. 6 we show the scaling function for the set of data  $A = 12$ –197 that extends to the most negative values of  $\psi'$  reached, together with previous data on  $A = 4$  [25, 26] that also extend to rather large values of  $|\psi'|$ . Figure 6 shows that the scaling of the second kind extends out to the most negative values of the scaling variable presently accessible. At values of  $\psi' < -2$  the scaling function seems to drop more rapidly with increasing  $|\psi'|$ , a feature that at present is not yet understood; however, we continue to observe very high quality scaling of the second kind.

We have mentioned in the previous section that superscaling in terms of the variables  $\psi'$  and  $\Upsilon$  (see Eq. (15)) can be expected to be quite similar; data that scale in one variable can be expected to scale in the other one as well. As an example for this we show in Fig. 7 the data of Fig. 3 in terms of  $f(\Upsilon)$ . In this

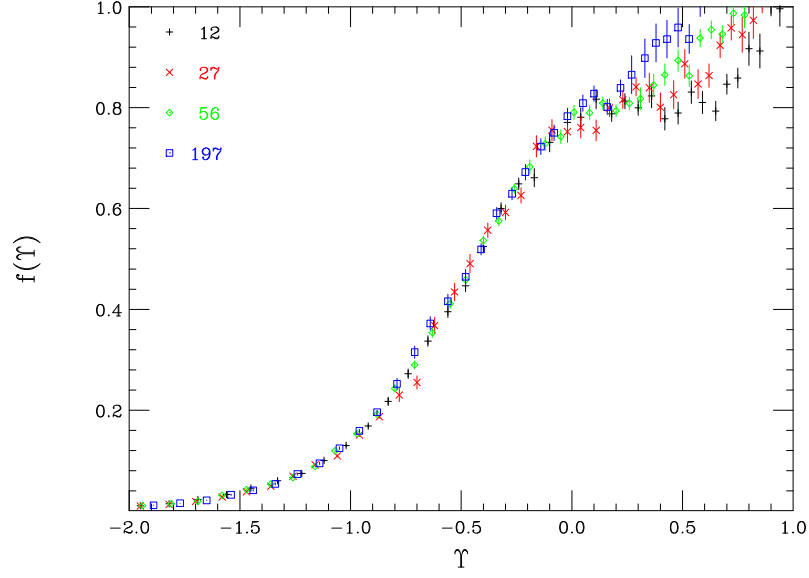


Figure 7: Scaling function  $f(\Upsilon)$  for nuclei  $A = 12$ – $197$  at  $3.6$  GeV energy and  $16$  degrees scattering angle as a function of the scaling variable  $\Upsilon$ .

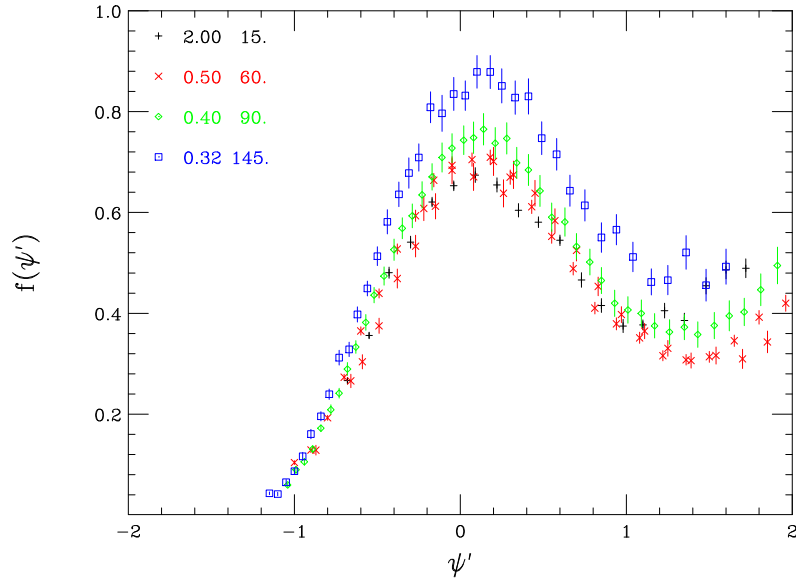


Figure 8: Scaling function for  $^{12}\text{C}$  at approximately constant  $q \approx 500$  MeV/c, but varying angle. The energies (in GeV) and angles (in degrees) of the different data sets are identified in the plot.



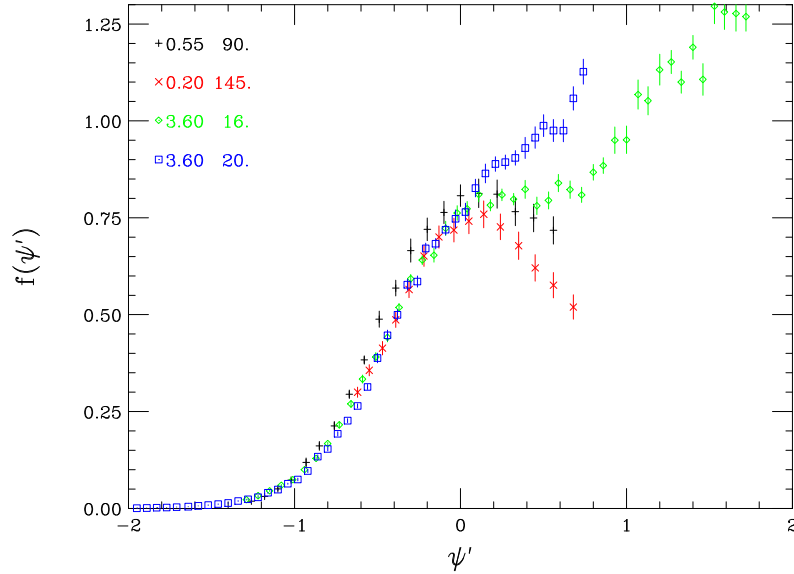


Figure 9: Scaling function for  $^{12}\text{C}$  and roughly constant ratio of the longitudinal and transverse e-p elastic cross section, as a function of the momentum transfer  $q$ .

paper we have concentrated on  $\psi'$  rather than  $\Upsilon$  since the former is more directly related to the RFG model that motivated superscaling in the first place, and that allowed us to introduce  $k_F$  as a physical scale used to define a dimensionless scaling variable. In the previous section we have given the relation between  $\Upsilon$  and  $\psi'$ , pointing out the difference in the treatment of the distribution in missing-energy which distinguishes the two scaling variables. The results show that, at the large values of  $q$  and  $\omega$  of interest here, the scaling behavior may be analyzed in terms of either variable.

In order to locate the origin of non-scaling when all kinematics are considered together (Fig. 2), for one nucleus ( $^{12}\text{C}$ ) we have selected data sets corresponding to roughly constant momentum transfer  $q$ , but variable scattering angle (due to the discrete nature of the sets of data available, the choice of sets at “constant  $q$ ” is only an approximate one). With increasing scattering angle, the ratio of the longitudinal to the total (longitudinal plus transverse) cross section decreases. For example, for e-p elastic scattering, which is characteristic of quasielastic electron-nucleus scattering, and for the momentum transfer  $q \approx 500 \text{ MeV}/c$  of Fig. 8, this ratio goes from 0.5 at the highest energy and smallest scattering angle down to less than 0.1 (i.e., the angle  $\chi_{TL}$  defined in the next section, which characterizes the TL ratio, goes from about  $45^\circ$  down to about  $15^\circ$  for the four sets of kinematics chosen). The rise of  $f(\psi')$  for decreasing longitudinal contribution clearly shows that the dominant piece responsible for non-scaling is the transverse one, as

expected from the dominantly transverse nature of  $\Delta$ -excitation and MEC. The violation of scaling is still comparatively small as the momentum transfer of the data in Fig. 8 is small.

Figure 9 gives a different cut through the data presently available. Here we plot sets of data with an approximately constant longitudinal/transverse ratio for the elastic e-p cross section, but varying momentum transfer  $q$  (here  $\chi_{TL}$  is roughly constant, typically within a few degrees of  $25^\circ$ ). The range of  $q$  covered here is 320 to 1120 MeV/c. Clearly, the non-scaling contribution at  $\psi' > 0$  rises rapidly with  $q$ . Part of this increase of the contribution at  $\psi' > 0$  originates from the fact that the quasielastic peak has a width that increases with  $q$ ; as a consequence, the overlap of the quasielastic response and the contribution from other processes grows with increasing  $q$ . This effect is not immediately obvious when looking at the representation in Fig. 9 as the use of the scaling variable  $\psi'$  removes this increase for the quasielastic contribution. It arises partially because pion production (including via  $\Delta$  production) moves to the left with increasing  $q$  and so overlaps with the quasielastic peak (at  $\psi' = 0$ ). Other processes may also play a role, in particular those involving MEC (to which we briefly return in the next two sections) and eventually at high energies those involving deep inelastic electron-nucleon scattering. We note that, according to Fig. 8, these non-quasifree contributions are basically of transverse nature. This suggests going further and attempting to disentangle the L and T contributions to scaling — we proceed to do so in the next section.

## 4 Scaling of Separated Responses

The various ways of looking at sub-samples of the data discussed above show clearly that the violation of superscaling is basically the same as the one observed in conventional scaling applied to a single nucleus. The deviations from scaling observed in Fig. 2 can be understood in terms of the  $q$ - and L/T-dependence for a single nucleus. In particular, let us proceed to extend the formalism of Sec. 2 by writing longitudinal and transverse versions of Eq. (14). Starting from the cross section written in terms of the individual response functions  $R_L$  and  $R_T$ ,

$$\frac{d^2\sigma}{d\Omega_e d\omega} = \sigma_M [v_L R_L(\kappa, \lambda) + v_T R_T(\kappa, \lambda)], \quad (26)$$

we have from Eq. (14) that

$$F = \frac{v_L R_L + v_T R_T}{v_L G_L + v_T G_T}, \quad (27)$$

with  $G_{L,T}$  given in Eqs. (54). The longitudinal and transverse analogs of this equation are

$$F_L = \frac{R_L}{G_L}, \quad F_T = \frac{R_T}{G_T}. \quad (28)$$

As we shall see below, it proves useful to study the difference between these two quantities

$$\Delta F \equiv F_T - F_L. \quad (29)$$

If the reaction mechanism in the quasielastic region is strictly (quasifree) knockout of protons and neutrons, then one has  $F_L(\kappa, \psi) = F_T(\kappa, \psi) = F(\kappa, \psi)$ , namely, one has  $\Delta F(\kappa, \psi) = 0$ . In light of the discussions in the present work we might call this universality scaling of the *zeroth kind*.

The dimensionless analogs of Eq. (24) are given by

$$f_{L,T} \equiv k_F F_{L,T} \quad (30)$$

$$\Delta f \equiv k_F \Delta F = f_T - f_L. \quad (31)$$

The universality contained in the RFG model predicts that

$$f_L = f_T = f, \quad (32)$$

where the last is given in Eq. (25), and moreover that

$$\int d\psi f^{RFG}(\psi) = 1 + \frac{1}{20}\eta_F^2 + \dots, \quad (33)$$

which is closely related to the Coulomb sum rule [18].

It is convenient to express the relationship amongst the  $f$ 's (or the  $F$ 's) in the form

$$f \equiv \sin^2 \chi_{TL} f_L + \cos^2 \chi_{TL} f_T, \quad (34)$$

where the angle  $\chi_{TL}$  characterizes the TL content of the scattering ( $\chi_{TL} = 0^\circ \leftrightarrow$  all T;  $\chi_{TL} = 90^\circ \leftrightarrow$  all L). It is a solution to the equation

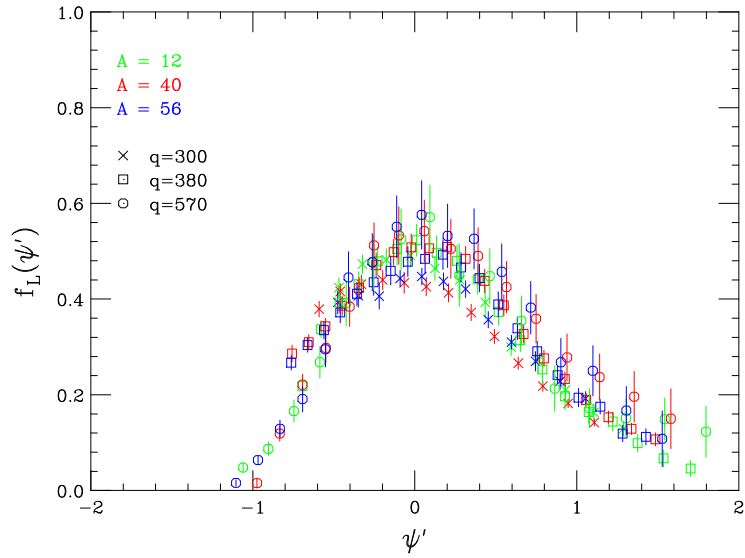
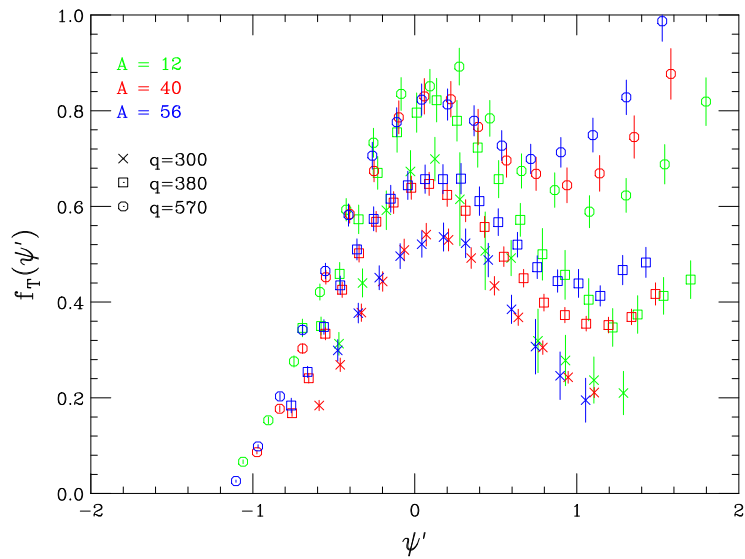
$$\tan^2 \chi_{TL} \equiv (v_L/v_T)(G_L/G_T) \quad (35)$$

$$\cong \frac{(\tilde{G}_E/\tilde{G}_M)^2}{\tau + 2\kappa^2 \tan^2 \theta_e/2}. \quad (36)$$

We thus have a direct relationship for  $\Delta f$  in terms of  $f$  and  $f_L$  (see below):

$$\Delta f = (f - f_L)/\cos^2 \chi_{TL}, \quad (37)$$

where this can be written in terms of Eqs. (35,36) using the fact that  $1/\cos^2 \chi_{TL} = 1 + \tan^2 \chi_{TL}$ . In the data sets considered in the previous section the angle  $\chi_{TL}$

Figure 10: Scaling function  $f_L(\psi')$  from the longitudinal response.Figure 11: Scaling function  $f_T(\psi')$  from the transverse response.

varies considerably: specifically, in Figs. 3, 5 and 7 it is within a few degrees of  $29^\circ$ ; in Fig. 4 within a few degrees of  $43^\circ$ ; in Fig. 6 within a few degrees of  $20^\circ$ ; while for Figs. 8 and 9 the values were stated earlier.

Scaling of the first kind of the longitudinal and transverse response functions has been studied some time ago by Finn *et al.* [44]. These authors found that, over the region  $q$  from 250 to 550 MeV/c, the longitudinal response of  $^{12}\text{C}$  showed good scaling, while the transverse response did not. More recently [36]  $\psi'$ -scaling of L and T responses was investigated for the case of  $^{40}\text{Ca}$ .

As pointed out above, the longitudinal and transverse contributions to the cross sections should — for quasielastic scattering in PWIA — also show scaling of the second kind, in fact to the same response function; see Eq. (32). In Figs. 10 and 11 we compare the scaling functions  $f_L(\psi')$  and  $f_T(\psi')$  obtained by Jourdan [45, 46] who performed a longitudinal/transverse separation of the data for selected nuclei and the lower momentum transfers ( $<580$  MeV/c) where enough data for such a separation are available. Within the error bars of the separated data the longitudinal response does scale to a universal curve, and as shown by Jourdan [45], the integral over this curve does fulfill the Coulomb sum rule (Eq. (33)). Figures 10 and 11 also show that the basic problem in quasielastic electron-nucleus scattering is the *excess in the transverse response* at large energy loss which grows rapidly with  $q$ . It is *not* a lack of strength in the longitudinal response, as was claimed by some of the earlier determinations of the longitudinal response.

Figures 10 and 11 also explain the behavior of  $f(\psi')$  found in the previous figures at larger  $q$ 's. A transverse contribution is clearly present which, up to  $\psi' \approx +0.6$ , has roughly the shape of the quasielastic peak. This leads to an excess of the transverse over the longitudinal strength without modifying the shape of the response in the region of the peak. For  $\psi' < +0.6$  scaling of the *second kind* is quite good, whereas scaling of the *first kind* is not. At larger  $\psi'$  a (likely different) non-scaling contribution comes in at the larger  $q$ , which is much more important for the heavier nuclei; that is, even scaling of the second kind is broken there.

In order to illustrate this point better, in Fig. 12 we show the *difference* between the transverse and longitudinal scaling functions,  $\Delta f(\psi')$  defined in Eq. (31).

As the longitudinal scaling functions for the different momentum transfers and mass numbers define an essentially universal curve (see Fig. 10), we have taken a bin-wise average of the data for the higher  $q$ 's of Fig. 10 in order to obtain the mean longitudinal response with smaller fluctuations. As the response at the lowest value of  $q \approx 300$  MeV/c is still subject to Pauli blocking, we use only the data at the higher  $q$ 's to determine this universal longitudinal response. Indeed, to the extent that one believes this to be *the* superscaled  $f_L$ , it is then

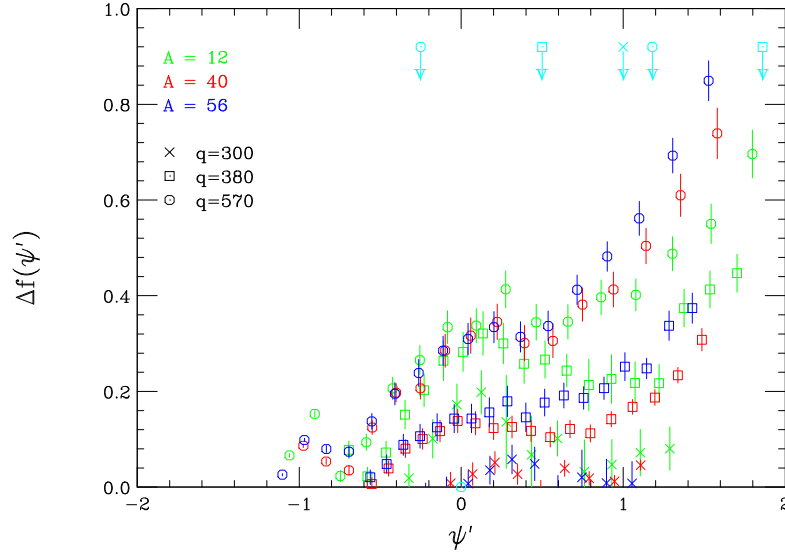


Figure 12: Difference between the transverse and longitudinal scaling functions,  $\Delta f(\psi')$ . The arrows indicate the values of  $\psi'$  for  $\pi$ -production on the free nucleon and the nucleus at the three values of  $q$ .

possible to use the unseparated function  $f$  for *any* nucleus with  $A \geq 4$  and *any* (large enough) momentum transfer via Eq. (37) to determine  $\Delta f$  and hence  $f_T$ . The difference in Fig. 12 shows that part of the excess transverse strength does indeed display a peak at the location of the maximum of the quasielastic response,  $\psi'=0$ . The strength at larger  $\psi'$ , corresponding to larger electron energy loss and of presumably different origin, rises rapidly with increasing  $q$ .

Much of the strength of  $\Delta f$  at  $\psi' < 0$  is below the threshold for pion production on a nucleus with  $A \geq 12$  (and even more so for quasifree production). This is shown by the arrows in Fig. 12 which indicate, for the various  $q$ 's, the position of the  $\pi$ -production threshold both on the nucleus and on the free nucleon — we consider the latter to be the more relevant one, since coherent production on the entire nucleus is expected to be very small. The presence of large excess transverse strength *below*  $\pi$ -threshold means that some other mechanism must be identified as its source. Various possibilities exist, for example, non-quasifree reactions in which the FSI are different for nucleon knockout via the L and T contributions of the electromagnetic current, cluster knockout and two-body MEC contributions; we return to touch upon some of these in the next section.

While the qualitative message of Fig. 12 is clear, we note that the numerical values of the difference in strength given there should be treated with some care. It is clear that some processes playing a role in accounting for the excess strength (for example, one-particle emission via MEC) arise from *coherent* contributions

to quasielastic scattering, and hence make any quantitative interpretation of  $\Delta f$  less straightforward than would be the case when only incoherent processes are present.

## 5 Discussion and Conclusions

We have analyzed the existing high-quality data on electron-nucleus quasielastic scattering for all nuclei  $A = 4$ –238. We observe that, upon use of the proper scaling variable  $\psi'$  (or, alternatively,  $\Upsilon = y/k_F$ ), the data on the low- $\omega$  side of the quasielastic peak ( $\psi'$  or  $\Upsilon < 0$ ) show *superscaling* behavior: the scaling functions are not only independent of momentum transfer, but coincide for the different  $A$  once the leading  $k_F$  dependence is removed in the manner discussed in this work. The former we call scaling of the *first kind* and the latter scaling of the *second kind*.

The main part of this work has been performed using the scaling variable  $\psi'$  introduced within the context of the RFG model as motivation for the definition of a dimensionless scaling variable using the Fermi momentum as a scale. We have also discussed the relationship between  $\psi'$  and the usual scaling variable  $y$ , and shown that the two variables, which integrate somewhat different initial-state physics, yield similar results. Indeed, the superscaling property is found in terms of both  $\psi'$  and  $\Upsilon$ .

The  $A$ -independence of the superscaling function actually is much better realized than the  $q$ -independence of the normal scaling; scaling of the first kind is known to be violated due to effects from FSI (mainly at very negative  $\psi'$ ) and MEC, pion production and excitation of internal degrees of freedom of the nucleon (mainly at  $\psi' > 0$ ). This observation of superscaling allows us to conclude that, in the integral sense reflected through inclusive scattering, different nuclei have a more or less universal spectral function (momentum distribution) once the obvious dependence on the Fermi momentum  $k_F$  is removed. This universality is not restricted to the region of the quasielastic peak ( $|\psi'| < 1$ ); the superscaling extends to larger values of  $|\psi'|$  and hence to large values of the nucleon momentum in the nucleus, a fact which may stem from the universal properties of nuclear spectral functions that arise from short-range N–N interactions insofar as they can lead to a scaling in terms of  $k/k_F$ .

Superscaling turns out to be particularly useful when dealing with the separated longitudinal and transverse responses. In quasielastic scattering for all large enough momentum transfers and all nuclear mass numbers  $A \geq 4$  both of these responses should scale to the *same* function to which the unseparated data also scale. In particular, to the extent that the limited scope of the available data permits a test to be made, we find that the *longitudinal* response does scale

to a universal curve, and that the integral of the superscaled result satisfies the Coulomb sum rule.

However, when using superscaling to investigate further the reasons that lead to the observed non-scaling at electron energy loss  $\omega' > |Q^2|/2m_N$  ( $\psi' > 0$ ) for individual nuclei, we find that the main problem resides in the *transverse* strength, which increases rapidly with increasing  $q$ , and less rapidly with increasing  $A$ . Some of the increase with  $q$  is clearly related to the increasing overlap of the quasielastic contribution with the  $\Delta$ -peak (which is predominantly transverse), the growing contribution of  $\pi$  production and at the highest energies deep-inelastic scattering. This cannot provide all of the excess in  $\Delta f$ , however, since it clearly occurs below threshold for meson production, as well as at higher energy loss.

Thus, the good quality of the scaling of the second kind is not entirely understood. Various sources for the excess transverse strength can be identified, ranging from FSI effects to contributions from MEC. The former could yield some T/L differences through spin-isospin many-body contributions arising from RPA correlations or effects involving correlated knockout of nucleon pairs (for instance, the  $^1S_0 \rightarrow ^3S_1 + ^3D_1$  channel is primarily transverse), although it is completely unclear what breaking of scaling of the first or second kinds might be produced and whether the transverse/longitudinal excess could be so explained. Indeed, for example, one can argue that some contributions such as those stemming from short-range FSI are reasonably A-independent. This is not the case for the contribution of MEC. For instance, the treatment of Van Orden and Donnelly [43] shows that the 2p-2h MEC superscaled response contains an additional dependence of approximately  $k_F^3$  and hence strongly breaks the second-kind scaling behavior. In fact, those calculations yielded a rather small 2p-2h contribution — which is consistent with what is observed. Other studies [47, 48] confirm this behavior. In particular, even calculations involving a dynamic  $\Delta$  propagator, such as those of Dekker et al. [47], while providing somewhat larger 2p-2h MEC contributions, do not provide so much that they disagree with the second kind scaling behavior (although note that for reasons we do not yet understand recent work [49] appears to be in conflict with the earlier treatments). Furthermore, it should be pointed out that MEC effects enter in the 1p-1h sector as well as in the 2p-2h sector. In [50] (and confirmed in [48]) it was seen that the former interfere destructively with the one-body contributions and therefore tend to lower the total 1p-1h transverse response — when all is added up the total MEC effect at and below the quasielastic peak is found to be rather small. Clearly the reasons for the good quality of the scaling of the second kind and the limits that may be imposed on processes such as MEC-mediated 2p-2h excitations certainly merit further theoretical investigation.

In summary, superscaling, when applied to these separated responses, allows



one in a particularly obvious way to make a point that recently has become increasingly clear: for inclusive electron-nucleus scattering the poorly understood contribution is the *transverse* one, and not the longitudinal one as was usually claimed before the work of Jourdan [45] in which reliable values for the longitudinal response were extracted.

## Acknowledgements

The authors would like to thank J. Jourdan for providing the scaling functions for the longitudinal and transverse responses and C.F. Williamson for useful discussions during the course of this work.

This work was supported in part by funds provided by the U.S. Department of Energy under cooperative research agreement #DF-FC02-94ER40818, and by the Swiss National Science Foundation.

## Appendix

### Kinematical Relationships

Using Eq. (1) it may be shown that when  $\mathcal{E} = 0$  (its smallest value) the minimum and maximum values of the missing-momentum occur at  $|y|$  and  $Y$ , respectively, where [1]

$$y = \frac{1}{2W^2} \left\{ (M_A^0 + \omega) \sqrt{W^2 - (M_{A-1}^0 + m_N)^2} \sqrt{W^2 - (M_{A-1}^0 - m_N)^2} - q \left[ W^2 + (M_{A-1}^0)^2 - m_N^2 \right] \right\} \quad (38)$$

$$Y = \frac{1}{2W^2} \left\{ (M_A^0 + \omega) \sqrt{W^2 - (M_{A-1}^0 + m_N)^2} \sqrt{W^2 - (M_{A-1}^0 - m_N)^2} + q \left[ W^2 + (M_{A-1}^0)^2 - m_N^2 \right] \right\} \quad (39)$$

with as usual  $W = \sqrt{(M_A^0 + \omega)^2 - q^2}$ . The variable  $y = y(q, \omega)$  may be used together with  $q$  to replace the pair of variables  $(q, \omega)$  and is well-suited to quasielastic electron scattering, since the quasielastic peak occurs near  $y = 0$ , with  $y < 0$  corresponding to the so-called “ $y$ -scaling region” which is the focal point of this work, whereas  $y > 0$  corresponds to the resonance region and beyond to deep-inelastic scattering. Expanding in inverse powers of the daughter mass one has

$$y = y_\infty \left[ 1 - \left( \frac{\sqrt{m_N^2 + (q + y_\infty)^2}}{q + y_\infty} \right) \frac{y_\infty}{2M_{A-1}^0} + \mathcal{O}[(M_{A-1}^0)^{-2}] \right], \quad (40)$$

where  $y_\infty$  is given in Eq. (2). The upper limit may similarly be expanded for large  $M_{A-1}^0$ , yielding

$$Y \cong 2q \left[ 1 - \frac{\sqrt{m_N^2 + (q + y_\infty)^2}}{M_{A-1}^0} \right] + y. \quad (41)$$

Another useful relationship needed in some of the discussions presented in Sec. 2 is that for the maximum value of missing-energy allowed for given  $(q, \omega)$  and given missing-momentum  $p$ . One finds that  $\mathcal{E}$ , which is essentially the missing-energy minus the separation energy  $E_s$ , has as its maximum value

$$\begin{aligned} \mathcal{E}_M(q, y; p) &= \sqrt{m_N^2 + (q + y)^2} - \sqrt{m_N^2 + (q - p)^2} \\ &\quad + \sqrt{(M_{A-1}^0)^2 + y^2} - \sqrt{(M_{A-1}^0)^2 + p^2} \\ \xrightarrow{M_{A-1}^0 \rightarrow \infty} &\sqrt{m_N^2 + (q + y)^2} - \sqrt{m_N^2 + (q - p)^2} - (p^2 - y^2)/2M_{A-1}^0 \\ \xrightarrow{q \rightarrow \infty} &(p + y) - \left( \sqrt{(M_{A-1}^0)^2 + p^2} - \sqrt{(M_{A-1}^0)^2 + y^2} \right) \\ \xrightarrow{M_{A-1}^0 \rightarrow \infty} &(p + y) - (p^2 - y^2)/2M_{A-1}^0. \end{aligned} \quad (42)$$

In the main part of the paper we employ only the  $M_{A-1} \rightarrow \infty$  limit as in Eqs. (6,7).

All of the kinematic relationships given above do not depend on the choice of dynamical model beyond the assumption of nucleon knockout.

## PWIA and the cc1 Off-shell Prescription

If following common practice one invokes the PWIA for the reaction, then a nucleon of energy

$$E(p, \mathcal{E}) = M_A^0 - \sqrt{(M_{A-1}^0)^2 + p^2} - \mathcal{E} \quad (43)$$

and momentum  $p$  is struck by the virtual photon and is ejected from the nucleus as a plane-wave (on-shell) with energy  $E_N$  and momentum  $p_N$ . The kinematics of the reaction require the struck nucleon to be off-shell; that is,  $E \neq \bar{E}$ , where  $\bar{E} \equiv (m_N^2 + p^2)^{1/2}$ . In fact the off-shellness may be characterized by the quantity

$$\begin{aligned} \rho(p, \mathcal{E}) &\equiv \frac{\bar{E} - E}{2m_N} \\ &= \frac{1}{2m_N} \left[ \left( \sqrt{m_N^2 + p^2} - m_N \right) + \left( \sqrt{(M_{A-1}^0)^2 + p^2} - M_{A-1}^0 \right) \right. \\ &\quad \left. + \mathcal{E} + E_s \right] \geq E_s/2m_N. \end{aligned} \quad (44)$$

In PWIA the cross section is given as the product of the half-off-shell single-nucleon cross section and the nuclear spectral function  $\tilde{S}(p, E)$  which gives the probability that a nucleon of momentum  $p$  and energy  $E$  is found in the nuclear ground state. We may then write  $\tilde{S}$  as a function of  $(p, \mathcal{E})$ .

For the single-nucleon cross section it is common practice to use the cc1 prescription of De Forest [16]. Then, integrating over azimuthal angles, summing over particles while assuming that the spectral function does not differ for protons and neutrons, and including the kinematic factor  $E_N/q$  with  $E_N = ((\mathbf{q} + \mathbf{p})^2 + m_N^2)^{1/2}$  (see [1]), one obtains the following for the single-nucleon cross section:

$$\tilde{\sigma}_{eN}(q, \omega; p, \mathcal{E}) \equiv \sigma_M [v_L \tilde{w}_L + v_T \tilde{w}_T], \quad (45)$$

with  $\sigma_M$  the Mott cross section and  $v_{L,T}$  the usual Rosenbluth kinematical factors, where the longitudinal (L) and transverse (T) cc1 contributions may be written:

$$\begin{aligned} \tilde{w}_L(q, \omega; p, \mathcal{E}) &= \frac{1}{2\kappa\sqrt{1+\eta^2}} \left(\frac{\kappa^2}{\bar{\tau}}\right) [\tilde{G}_E^2 + \delta^2(\tilde{W}_2 + \Delta\tilde{W}_1) \\ &\quad + (1 + \bar{\tau})\Delta\tilde{W}_1 + (1 + \tau)\Delta\tilde{W}_2] \\ \tilde{w}_T(q, \omega; p, \mathcal{E}) &= \frac{1}{2\kappa\sqrt{1+\eta^2}} [2\bar{\tau}\tilde{G}_M^2 + \delta^2(\tilde{W}_2 + \Delta\tilde{W}_1)]. \end{aligned} \quad (46)$$

Here we employ dimensionless variables  $\kappa \equiv q/2m_N$ ,  $\lambda \equiv \omega/2m_N$ ,  $\tau \equiv \kappa^2 - \lambda^2 > 0$ , where  $\omega = E_N - E$ . The cc1 prescription introduces the energy  $\bar{E}$  given above and hence the ‘‘equivalent on-shell energy transfer’’  $\bar{\omega} = E_N - \bar{E}$ , with  $\bar{\lambda} \equiv \bar{\omega}/2m_N$  and  $\bar{\tau} \equiv \kappa^2 - \bar{\lambda}^2$ . We have also defined  $\eta \equiv p/m_N$ , where then  $\bar{E}/m_N = (1 + \eta^2)^{1/2}$ , and used the fact that:

$$\delta^2 \equiv \frac{\bar{\tau}}{\kappa^2} \left(\frac{E_N + \bar{E}}{2m_N}\right)^2 - (1 + \bar{\tau}) \quad (47)$$

$$= \frac{\bar{\tau}}{\kappa^2} [2\bar{\lambda}(\sqrt{1 + \eta^2} - 1) + \eta^2] - \left(\frac{\bar{\lambda} - \bar{\tau}}{\kappa}\right)^2, \quad (48)$$

where the relationship  $(E_N + \bar{E})/2m_N = \bar{\lambda} + \sqrt{1 + \eta^2}$  has been used to obtain the result in Eq. (48). The terms containing  $\delta^2$  as a factor enter because the struck nucleon is moving and contribute whether or not the nucleon is off-shell. As discussed in the main text,  $\eta$  is typically small; therefore the first term in Eq. (48) is very small, being of order  $\eta^2$ . For the second term in this equation we can use as an estimate Eq. (16) and find that its contribution is also very small, being of order  $\eta_F^2$ . Thus the terms in Eqs. (46) containing the factor  $\delta^2$  are all seen to be very small.

The single-nucleon form factors enter Eqs. (46) in the following combinations:

$$\tilde{G}_E^2(\tau) \equiv ZG_{Ep}^2 + NG_{En}^2$$

$$\begin{aligned}
\tilde{G}_M^2(\tau) &\equiv ZG_{Mp}^2 + NG_{Mn}^2 \\
\Delta\tilde{G}(\tau) &\equiv ZG_{Ep}G_{Mp} + NG_{En}G_{Mn}
\end{aligned}
\tag{49}$$

where  $G_{Ep,n}$  and  $G_{Mp,n}$  are the familiar Sachs form factors and are functions only of  $\tau$ , and then:

$$\begin{aligned}
\tilde{W}_1(\tau) &\equiv \tau\tilde{G}_M^2 \\
\tilde{W}_2(\tau) &\equiv \frac{1}{1+\tau}[\tilde{G}_E^2 + \tau\tilde{G}_M^2] \\
\Delta\tilde{W}_1(\tau, \bar{\tau}) &= \frac{\bar{\tau} - \tau}{(1+\tau)^2} [\tilde{G}_E^2 + \tilde{G}_M^2 - 2\Delta\tilde{G}] \\
\Delta\tilde{W}_2(\tau, \bar{\tau}) &= \frac{\bar{\tau} - \tau}{(1+\tau)^2} [\tilde{G}_E^2 - \tilde{G}_M^2].
\end{aligned}
\tag{50}$$

The form given here for the cc1 prescription is different from the usual one [16], having been rearranged to bring out the strong resemblance to the on-shell form discussed below. Note that, when a nucleon is moving but on-shell, since  $\tau = \bar{\tau}$  the last two responses are zero,  $\Delta\tilde{W}_{1,2} = 0$ . That also implies, as expected, that no terms of the form  $G_E G_M$  coming from  $\Delta\tilde{G}$  in Eq. (50) can occur when on-shell, although they do for the cc1 off-shell prescription. Finally, note that these off-shell effects are all proportional to  $\bar{\tau} - \tau$  which may be written

$$\bar{\tau} - \tau = \rho(2\lambda - \rho) \tag{51}$$

using Eq. (44).

## Scaling in the RFG Model

We end this Appendix by collecting some of the exact expressions involved in studies of the RFG model (see also [12, 18]). First the  $\psi$ -scaling variable is fully given by

$$\psi = \frac{1}{\sqrt{\xi_F}} \frac{\lambda - \tau}{\sqrt{(1+\lambda)\tau + \kappa\sqrt{\tau(1+\tau)}}}, \tag{52}$$

where  $\xi_F = \sqrt{1 + \eta_F^2} - 1$  and  $\eta_F = k_F/m_N$  are the dimensionless Fermi kinetic energy and momentum, respectively. Approximations to this quantity were employed in the main part of the paper for simplicity (see Eqs. (10,12)), although computations were done with the full expression.

The exact RFG analog of Eq. (3) is:

$$F(\kappa, \psi) \equiv \frac{d^2\sigma/d\Omega_e d\omega}{\sigma_M[v_L G_L(\kappa, \lambda) + v_T G_T(\kappa, \lambda)]}, \tag{53}$$

where we have made use of the usual lepton kinematical factors  $v_L$  and  $v_T$  and on-shell single-nucleon responses  $G_L$  and  $G_T$  (see [18], and also [51, 52])

$$\begin{aligned}
G_L(\kappa, \lambda) &= \frac{(\kappa^2/\tau)[\tilde{G}_E^2 + \tilde{W}_2\Delta]}{2\kappa[1 + \xi_F(1 + \psi^2)/2]} \\
&= \frac{\kappa}{2\tau}\tilde{G}_E^2 + \mathcal{O}[\eta_F^2] \\
G_T(\kappa, \lambda) &= \frac{2\tau\tilde{G}_M^2 + \tilde{W}_2\Delta}{2\kappa[1 + \xi_F(1 + \psi^2)/2]} \\
&= \frac{\tau}{\kappa}\tilde{G}_M^2 + \mathcal{O}[\eta_F^2].
\end{aligned} \tag{54}$$

Here [12]

$$\begin{aligned}
\Delta &= \xi_F(1 - \psi^2) \left[ \frac{\sqrt{\tau(1 + \tau)}}{\kappa} + \frac{1}{3}\xi_F(1 - \psi^2)\frac{\tau}{\kappa^2} \right] \\
&= \frac{1}{2}(1 - \psi^2)\eta_F^2 + \mathcal{O}[\eta_F^3].
\end{aligned} \tag{55}$$

The above approximations yield the expressions used in the main part of the paper (see Eq. (14)). Note that the on-shell limits of Eqs. (46) immediately give the behavior seen in Eqs. (54), as they should.

## References

- [1] D. Day, J.S. McCarthy, T.W. Donnelly, and I. Sick. *Ann. Rev. Nucl. Part. Sci.* **40**, 357 (1990).
- [2] Geoffrey B. West. *Phys. Rep.* **18**, 263 (1975).
- [3] R.A. Bonham and H.F. Wellenstein. *McGraw-Hill, ed. B. Williams*, page 234 (1977).
- [4] P.C. Hohenberg and P.M. Platzman. *Phys. Rev.* **152**, 198 (1966).
- [5] J.I. Friedman and H.W. Kendall. *Ann. Rev. Nucl. Sci.* **22**, 203 (1972).
- [6] W. Czyz and K. Gottfried. *Ann. of Phys.* **21**, 47 (1963).
- [7] Y. Kawazoe, G. Takeda, and H. Matsuzaki. *Prog. Theo. Phys.* **54**, 1394 (1975).
- [8] I. Sick, D. Day, and J.S. McCarthy. *Phys. Rev. Lett.* **45**, 871 (1980).

- [9] E. Pace and G. Salme. *Phys. Lett.* **110B**, 411 (1982).
- [10] C. Ciofi degli Atti, E. Pace, and G. Salme. *Phys. Lett.* **B127**, 303 (1983).
- [11] O. Benhar, A. Fabrocini, S. Fantoni, G.A. Miller, V.R. Pandharipande, and I. Sick. *Phys. Rev.* **C44**, 2328 (1991).
- [12] W.M. Alberico, A. Molinari, T.W. Donnelly, E.L. Kronenberg, and J.W. Van Orden. *Phys. Rev.* **C38**, 1801 (1988).
- [13] T. W. Donnelly and I. Sick. *Phys. Rev. Lett.* **82**, 3212 (1999).
- [14] R.R. Whitney, I. Sick, J.R. Ficenece, R.D. Kephart, and W.P. Trower. *Phys. Rev.* **C9**, 2230 (1974).
- [15] J. Arrington, C.S. Armstrong, T. Averett, O. Baker, L. deBever, C. Bochna, W. Boeglin, B. Bray, R. Carlini, G. Collins, C. Cothran, D. Crabb, D. Day, J. Dunne, D. DUTTA, R. Ent, B. Fillipone, A. Honegger, E. Hughes, J. Jensen, J. Jourdan, C. Keppel, D. Koltenuk, R. Lindgren, A. Lung, D. Mack, J. McCarthy, R. McKeown, D. Meekins, J. Mitchell, H. Mkrtchyan, G. Niculescu, T. Petitjean, O. Rondon, I. Sick, C. Smith, B. Tesburg, W. Vulcan, S. Wood, C. Yan, J. Zhao, and B. Zihlmann. *Phys. Rev. Lett.* **82**, 2056 (1999).
- [16] T. de Forest. *Nucl. Phys.* **A392**, 232 (1983).
- [17] G. Hoehler, E. Pietarinen, I. Sabba-Stefanescu, F. Borkowski, G.G. Simon, V.H. Walther, and R.D. Wendling. *Nucl. Phys.* **B114**, 505 (1976).
- [18] M.B. Barbaro, R. Cenni, A. DePace, T.W. Donnelly, and A. Molinari. *Nucl. Phys.* **A643**, 137 (1998).
- [19] R. Cenni, T.W. Donnelly, and A. Molinari. *Phys. Rev.* **C56**, 276 (1997).
- [20] A. Zghiche, J.F. Daniel, M. Bernheim, M. Brussel, G.P. Capitani, E. de Sanctis, S. Frullani, F. Garibaldi, A. Gerard, J.M. Le Goff, A. Magnon, C. Marchand, Z.E. Meziani, J. Morgenstern, J. Picard, D. Reffay-Pikeroen, M. Traini, S. Turck-Chieze, and P. Vernin. *Nucl. Phys.* **A572**, 513 (1994).
- [21] S.A. Dytman, A.M. Bertstein, K.I. Blomquist, T.J. Pavel, B.P. Quinn, R. Altamus, J.S. McCarthy, G.H. Mechtel, T.S. Ueng, and R.R. Whitney. *Phys. Rev.* **C38**, 800 (1988).
- [22] Z.-E. Meziani, J.P. Chen, D. Beck, G. Boyd, L.M. Chinitz, D.B. Day, L.C. Dennis, G.E. Dodge, B.W. Fillipone, K.L. Giovanetti, J. Jourdan, K.W. Kemper, T. Koh, W. Lorenzon, J.S. McCarthy, R.D. McKeown, R.G. Milner,

- R.C. Minehart, J. Morgenstern, J. Mougey, D.H. Potterveld, O.A. Rondon-Aramayo, R.M. Sealock, I. Sick, L.C. Smith, S.T. Thornton, R.C. Walker, and C. Woodward. *Phys. Rev. Lett.* **69**, 41 (1992).
- [23] R.M. Sealock, K.L. Giovanetti, S.T. Thornton, Z.E. Meziani, O.A. Rondon-Aramayo, S. Auffret, J.-P. Chen, D.G. Christian, D.B. Day, J.S. McCarthy, R.C. Minehart, L.C. Dennis, K.W. Kemper, B.A. Mecking, and J. Morgenstern. *Phys. Rev. Lett.* **62**, 1350 (1989).
- [24] K.F. vanReden, C. Alcorn, S.A. Dytman, B. Lowry, B.P. Quinn, D.H. Beck, A.M. Bernstein, K.I. Blomqvist, G. Dodson, J. Flanz, G. Retzlaff, C.P. Sargent, W. Turchinez, M. Farkondeg, J.S. McCarthy, T.S. Ueng, and R.R. Whitney. *Phys. Rev.* **C41**, 1084 (1990).
- [25] D. Day, J.S. McCarthy, Z.E. Meziani, R. Minehart, R. Sealock, S.T. Thornton, J. Jourdan, I. Sick, B.W. Filippone, R.D. McKeown, R.G. Milner, D.H. Potterveld, and Z. Szalata. *Phys. Rev.* **C48**, 1849 (1993).
- [26] S. Rock, R.G. Arnold, B.T. Chertok, Z.M. Szalata, D. Day, J.S. McCarthy, F. Martin, B.A. Mecking, I. Sick, and G. Tamas. *Phys. Rev.* **C26**, 1592 (1982).
- [27] P. Barreau, M. Bernheim, M. Brussel, G.P. Capitani, J. Duclos, J.M. Finn, S. Frullani, F. Garibaldi, D. Isabelle, E. Jans, J. Morgenstern, J. Mougey, D. Royer, B. Saghai, E. de Sanctis, I. Sick, D. Tarnowski, S. Turck-Chieze, and P.D. Zimmermann. *Nucl. Phys.* **A358**, 287 (1981).
- [28] P. Barreau, M. Bernheim, J. Duclos, J.M. Finn, Z. Meziani, J. Morgenstern, J. Mougey, D. Royer, B. Saghai, D. Tarnowski, S. Turck-Chieze, M. Brussel, G.P. Capitani, E. de Sanctis, S. Frullani, F. Garibaldi, D.B. Isabelle, E. Jans, I. Sick, and P.D. Zimmermann. *Nucl. Phys.* **A402**, 515 (1983).
- [29] D.T. Baran, B.F. Filippone, D. Geesaman, M. Green, R.J. Holt, H.E. Jackson, J. Jourdan, R.D. McKeown, R.G. Milner, J. Morgenstern, D.H. Potterveld, R.E. Segel, P. Seidl, R.C. Walker, and B. Zeidman. *Phys. Rev. Lett.* **61**, 400 (1988).
- [30] J.S. O'Connell, W.R. Dodge, Jr. J.W. Lightbody, X.K. Maruyama, J.O. Adler, K. Hansen, B. Schroeder, A.M. Bernstein, K.I. Blomqvist, B.H. Cottman, J.J. Comuzzi, R.A. Miskimen, B.P. Quinn, J.H. Koch, and N. Ohtsuka. *Phys. Rev.* **C35**, 1063 (1987).
- [31] F.H. Heimlich, J. Obberling, J. Moritz, K.H. Schmidt, D. Wegener, D. Zeller, J.K. Bienlein, J. Bleckwenn, and H. Dinter. *Nucl. Phys.* **A231**, 509 (1974).

- [32] M Anghinolfi, M. Battalieri, N. Bianchi, R. Cenni, P. Corvisiero, A. Fantoni, P. LeviSandri, A. Longhi, V. Lucherini, V.I. Mokeev, V. Muccifora, E. Polli, A. Reolon, G. Ricco, M. Ripani, P. Rossi, S. Simula, M. Taiuti, A. Teglia, and A. Zucchatti. *Nucl. Phys.* **A602**, 405 (1996).
- [33] M. Deady, C.F. Williamson, J. Wong, P.D. Zimmerman, C. Blatchley, J.M. Finn, J. LeRose, P. Sioshans, R. Altemus, J.S. McCarthy, and R.R. Whitney. *Phys. Rev.* **C33**, 1897 (1986).
- [34] Z. Meziani, P. Barreau, M. Bernheim, J. Morgenstern, S. Turck-Chieze, R. Altemus, J. McCarthy, L.J. Orphanos, R.R. Whitney, G.P. Capitani, E. DeSanctis, S. Frullani, and F. Garibaldi. *Phys. Rev. Lett.* **54**, 1233 (1985).
- [35] T.C. Yates, C.F. Williamson, W.M. Schmitt, M. Osborn, M. Deady, P. Zimmerman, C.C. Blatchley, K. Seth, M. Sarmiento, B. Barker, Y. Jin, L.E. Wright, and D.S. Onley. *Phys. Lett.* **B312**, 382 (1993).
- [36] C.F. Williamson, T.C. Yates, W.M. Schmitt, M. Osborn, M. Deady, P.D. Zimmerman, C.C. Blatchley, K.K. Seth, M. Sarmiento, B. Parker, Y. Jin, L.E. Wright, and D.S. Onley. *Phys. Rev.* **C56**, 3152 (1997).
- [37] R. Altemus, A. Cafolla, D. Day, J.S. McCarthy, R.R. Whitney, and J.E. Wise. *Phys. Rev. Lett.* **44**, 965 (1980).
- [38] A. Hotta, P.J. Ryan, H. Ogino, B. Parker, G.A. Peterson, and R.P. Singhal. *Phys. Rev.* **C30**, 87 (1984).
- [39] J.P. Chen, Z.E. Meziani, G. Boyd, L.M. Chinitz, D.B. Day, L.C. Dennis, G. Dodge, B.W. Filippone, K.L. Giovanetti, J. Jourdan, K.W. Kemper, T. Koh, W. Lorenzon, J.S. McCarthy, R.D. McKeown, R.G. Milner, R.C. Minehart, J. Morgenstern, J. Mougey, D.H. Potterveld, O.A. Rondon-Aramayo, R.M. Sealock, L.C. Smith, S.T. Thornton, R.C. Walker, and C. Woodward. *Phys. Rev. Lett.* **66**, 1283 (1991).
- [40] C.C. Blatchley, J.J. leRose, O.E. Pruet, P.D. Zimmerman, C.F. Williamson, and M. Deady. *Phys. Rev.* **C34**, 1243 (1986).
- [41] M. Baldo, I. Bombaci, G. Giansiracusa, U. Lombardo, C. Mahaux, and R. Sartor. *Phys. Rev.* **C41**, 1748 (1990).
- [42] O. Benhar, A. Fabrocini, S. Fantoni, and I. Sick. *Nucl. Phys.* **A579**, 493 (1994).
- [43] J.W. Van Orden and T.W. Donnelly. *Ann. Phys.* **131**, 451 (1981).



- [44] J.M. Finn, R.W. Lourie and B.H. Cottman. *Phys. Rev.* **C29**, 2230 (1984).
- [45] J. Jourdan. *Nucl. Phys.* **A603**, 117 (1996).
- [46] J. Jourdan. *priv. com.*
- [47] M.J. Dekker, P.J. Brussaard, and J.A. Tjon. *Phys. Rev.* **C49**, 2650 (1991).
- [48] J.E. Amaro, G. Co' and A.M. Lallena. *Nucl. Phys.* **A578**, 365 (1994).
- [49] V. Gadiyak and V. Dmitriev. *Nucl. Phys.* **A639**, 685 (1998).
- [50] W.M. Alberico, T.W. Donnelly and A. Molinari. *Nucl. Phys.* **A512**, 541 (1990).
- [51] J.E. Amaro, J.A. Caballero, T.W. Donnelly, A.M. Lallena, E. Moya de Guerra, and J.M. Udías. *Nucl. Phys.* **A602**, 263 (1996).
- [52] S. Jeschonnek and T.W. Donnelly. *Phys. Rev.* **C57**, 2439 (1998).